Adsorption Breakthrough Behavior: Unusual Effects and Possible Causes

Illam Park and Kent S. Knaebel
Dept. of Chemical Engineering, Ohio State University, Columbus, OH 43210

Adsorption of water vapor on silica gel, at influent humidities from 6 to 80% at 25 and 50°C, yielded breakthrough curves of unusual shapes. Breakthrough patterns varied from the expected sigmoidal shape at low humidity to a curve resembling the tangent function, but symmetric about the stoichiometric breakthrough time. Unusual shapes were found to be due to subtle combinations of Type-IV isotherm behavior and heat effects. A mathematical model was developed to simulate the performance. The results show that complex breakthrough behavior need not be ascribed to complicated causes (such as diffusion in bidisperse pores), which require multiparameter fitting of experimental data. In fact, the effects may be predicted from properties measured in simple independent experiments, though some care is required to account for the effects accurately.

Introduction

Fixed-bed adsorption has been used widely in separation and purification of gases and liquids. To design such an adsorption process, it is important to understand the thermodynamic and kinetic characteristics of the adsorbent and adsorbate(s). One way to grasp these characteristics is by examining the concentration-vs.-time curves of the effluent. These breakthrough curves are perhaps the most common basis for assessing the behavior of adsorbers. Breakthrough curves depend on bed geometry, operating conditions, transport properties, heat effects, and equilibrium adsorption isotherm(s). Only a few previous studies have dealt with *a priori* prediction of breakthrough curves for systems with complicated isotherms, as will be discussed in some detail. Others have assessed kinetic and/or other parameters (including heat effects) *a posteriori* (Lee and Cummings, 1967; Chase, 1984), which were oriented toward interpretation of various effects from breakthrough behavior.

Early on, it was realized that isotherm shape has a dramatic effect on breakthrough curves. Isotherms were categorized according to the type of chromatogram obtained: convex-upward-shaped (favorable or Type-I) isotherms produced a constant pattern front, while convex-downward-shaped (unfavorable or Type-II) formed a proportional pattern. When mass transfer resistances are eliminated, adsorption following a Type-I isotherm appears as a shock wave, that is, step-change, and its counterpart during desorption is a simple wave. Equilibrium-dominated phenomena cause the prominent effects of interest here, while dissipative effects due to heat- and mass-transfer resistances do more to disguise those effects. To emphasize those aspects in this article, the breakthrough pattern under favorable or unfavorable conditions is referred to as a shock wave or simple wave, respectively, even though the actual shapes are ablated.

These isotherm shapes were the basis for interpretation of classical breakthrough curves by Glueckauf (1945, 1947, 1964). The realm of interpretation was expanded to account for other effects such as diffusion, dispersion, and reaction kinetics (for example, Chase, 1984). Many adsorbents and adsorbates, however, exhibit more complicated isotherm shapes due to pore-filling, complexation, or binding anomalies. Examples range from the mundane combination of silica gel and water vapor to esoteric adsorbents having functionalities for specific biomolecules (Whitley et al., 1990). Such applications may be categorized via classical types of isotherms, such as Type-IV, which has two inflections, while Type I has none. All systems become more complex when heat effects are significant.

The experimental system considered here is water vapor (in air) adsorbed on silica gel. Adsorption equilibrium and fixed-bed breakthrough behavior of that system were studied by Lee and Cummings (1967) and by Carter and Barrett (1973). They show the potential problems of explaining observed phenom-

Correspondence concerning this article should be addressed to K. S. Knaebel.

ena through a mathematical model: the former lumped heat- and mass-transfer effects into an effective mass-transfer coefficient; the latter missed the subtleties in breakthrough behavior by using a linear isotherm fit.

Ruthven et al. (1975) developed a simple model to calculate breakthrough curves and corresponding temperature profiles, and then validated it with various hydrocarbons adsorbed on 5A zeolite. Basmadjian (1980a,b) presented graphical methods for predicting the shape of isothermal and adiabatic breakthrough curves, while accounting for intraparticle diffusion. His approach showed that basic data can be used to predict complicated adsorption behavior. Frey (1990) examined criteria for existence of coherent discontinuities. His approach was to ignore all dissipative effects, such as film diffusion, intraparticle diffusion, and axial dispersion. In so doing, he obtained analytic solutions to the governing equations.

Farooq and Ruthven (1990a,b) analyzed heat effects and their influence on breakthrough patterns for systems exhibiting linear and Langmuir isotherms. They ignored all dissipative effects except for axial dispersion and solved the equations numerically. Ritter and Yang (1990) have also examined the effects of nonlinearity of the isotherm on breakthrough behavior, but they ignored heat effects. They considered the same basic types of isotherms, but incorporated hysteresis, rather than dispersion, into their analysis.

The purpose of this article is to understand the interactions of adsorption equilibrium, heat effects and mass transfer, and their roles in establishing the shape of breakthrough curves. In addition, the energy balance is shown to be relevant to both the breakthrough time and shape. Therefore, this article could be considered an extension of that by Ruthven et al. (1975); their observed breakthrough patterns were sigmoidal, while those observed here are complex. In fact, following conventional wisdom, they may have resulted from severe dispersion or intraparticle diffusion.

To find the causes of the unusual behavior, a mathematical model was used that ascertains values of the heat- and mass-transfer coefficients. With those estimates, breakthrough data obtained under other conditions were compared with the model predictions to validate the model. The model was then used to predict interstitial temperatures and compositions, which illustrated the onset and propagation of the unusual features evident in the breakthrough curves. Unusual features of those patterns, however, were due mainly to equilibrium and heat effects, even though some rounding was due to mass-transfer resistance.

Experimental Methods

Two kinds of experiments were conducted to measure equilibrium isotherms and breakthrough curves, respectively. Both sets of experiments were performed at about 25°C and 50°C and 1 atm. Table 1 lists all the experimental conditions and properties of the adsorbent. Figure 1 shows the three essential parts of the experimental equipment: (a) conditioned air source, (b) breakthrough apparatus, and (c) equilibrium adsorption isotherm apparatus. The air source was designed to supply air with constant relative humidity (RH) and constant flow rate for both types of experiments. Room air was compressed and cooled to the room temperature, and then passed through the mass-flow controller. The air was then split into two parts to be sent to a dryer and humidifier, respectively. The dry air (RH = 0%) and humid air (RH = 100%) streams were then mixed to produce air with a desired moisture content.

Table 1. Experimental Conditions

Adsorbent:	silica gel (Davison, PA-400) 12-28 mesh regenerated at full vacuum and 150°C overnight particle density, 2,100 kg/m^3
Adsorbate:	water vapor in air
Isotherm:	at 25 and 50°C, 1 bar net sample weight, 3.7137 and 4.8610 g
Breakthrough:	at 23-26°C, 1 bar Columns: (a) $D = 0.02362$ m, $L = 0.406$ m, $t = 0.89$ mm (b) $D = 0.02362$ m, $L = 0.200$ m, $t = 0.89$ mm (c) $D = 0.01339$ m, $L = 0.482$ m, $t = 1.25$ mm (d) $D = 0.02540$ m, $L = 0.300$ m, $t = 1.30$ mm net adsorbent weight, 0.005-0.138 kg bed porosity, 0.62-0.67 interstitial velocity, 0.112-0.125 m/s

The dryer was a fixed-bed adsorber comprising a glass column and activated alumina (Alcoa, F-200) regenerated at 250°C, which produced dry air (<0.1% RH). The humidifier comprised a glass column partly filled with distilled water. Air was admitted to a fritted distributor at the bottom of the column, which produced fine bubbles in the water and nearly 100% RH air. The rest of the column ensured that the water vapor was mixed well in the air. The feed air was controlled within ±1% RH by adjusting the flow ratio of the humid air to the dry air, with the two valves at the bottom.

To measure the equilibrium isotherm, an integral bed method was employed. Each end of the sample tube was sealed, hygrometer probes were inserted in both the influent and effluent lines, and the whole unit was surrounded by air at constant temperature (±0.2°C). The sample tube was filled with regenerated silica gel and weighed before it was exposed to the feed air. The experiment began when humid air was admitted to the tube. When the effluent humidity remained at the same humidity as the influent for more than an hour, the sample tube was taken off from the unit to determine the net weight of water vapor in silica gel. Afterwards, the tube was returned to the unit to ensure that no more uptake was possible. Once the steady state was achieved, it was assumed to coincide with equilibrium, and the RH of feed air was stepped up (for adsorption isotherms) or stepped down (for desorption isotherms).

For breakthrough experiments, two hygrometers and two pressure transducers were inserted before and after the adsorption column, respectively. In addition, a thermocouple was placed at the effluent end of the fixed bed of adsorbent. To prepare for an experiment, dried silica gel was weighed and packed in the column. The feed air at a constant relative humidity and at a constant flow rate, as the influent, was passed through the column, and the RH and the temperature of the effluent were read from the hygrometer at regular intervals. In this way, breakthrough curves were obtained at various RHs of the influent.

Experimental Results and Interpretation

Equilibrium properties

Figure 2 shows adsorption and desorption isotherms for

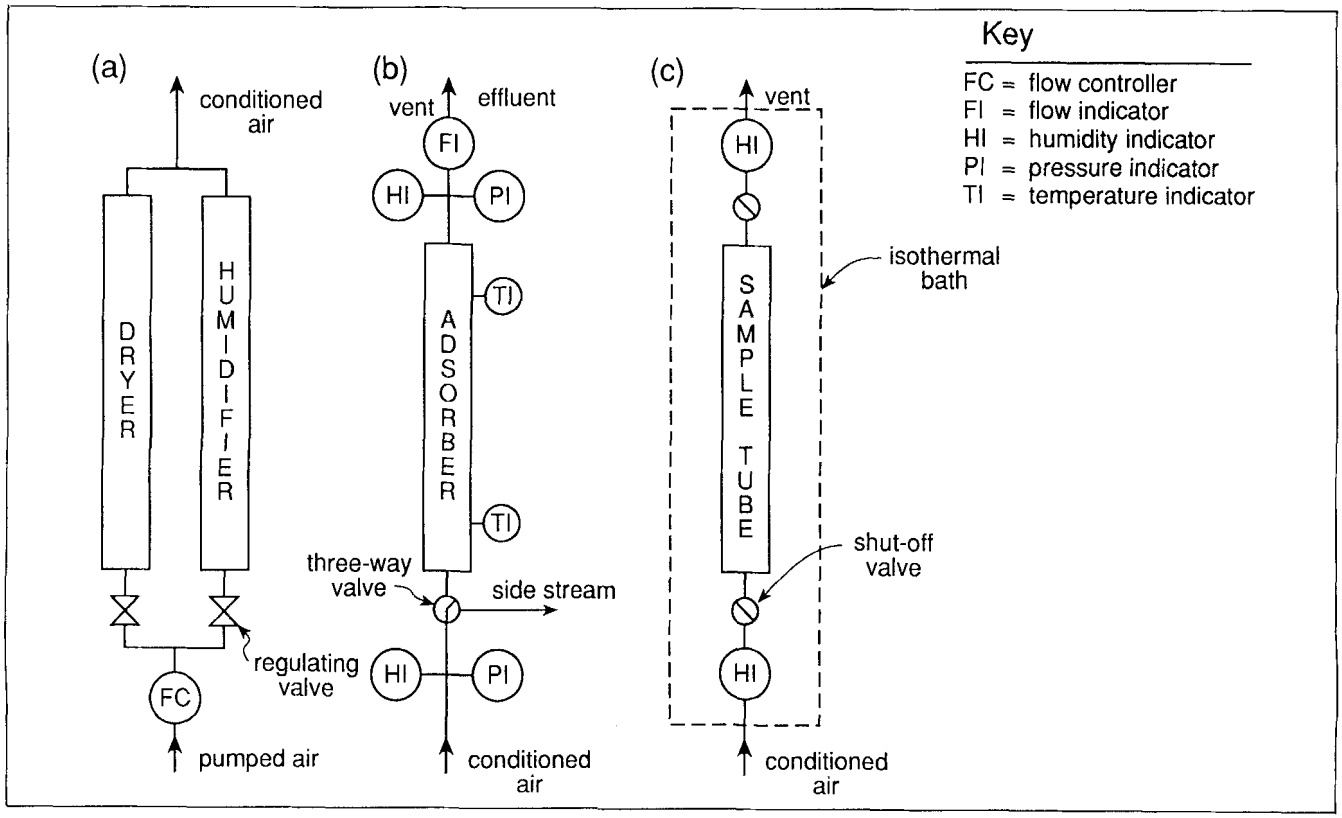

Figure 1. Experimental apparatus for: (a) conditioned air, (b) breakthrough, (c) equilibrium adsorption isotherm.

water vapor on silica gel (Davison, PA400) obtained at 25 and 50°C. Over the full range of relative humidity, the adsorption isotherms exhibit Type-IV behavior, and the results are close to the collective data given by van den Bulck (1990) for water vapor on regular density silica gel. The equilibrium uptake data for each temperature were fitted with both the Brunauer-Deming-Deming-Teller (1940) and Dubinin-Astakhov (1971) isotherm equations. The parameters are in Table 2.

The adsorbent-adsorbate interactions observed, as the relative humidity increased, may be explained as follows. The adsorption isotherm at 25°C, for instance, begins with gradual

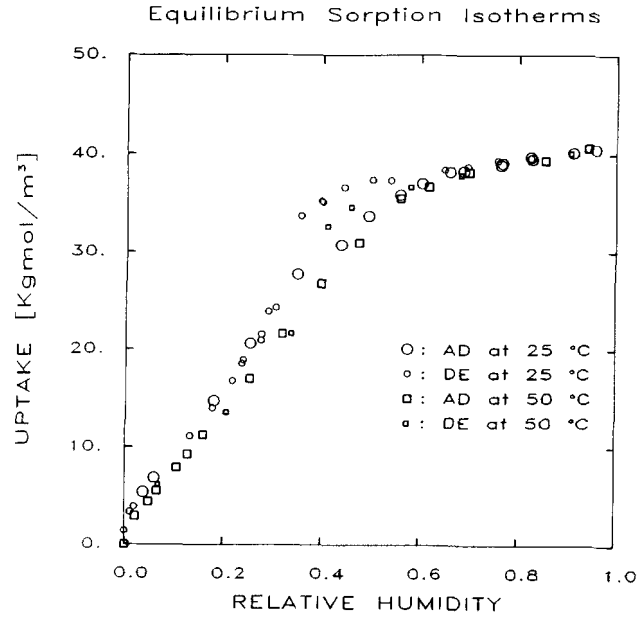

Figure 2. Equilibrium isotherms of water vapor on silica gel at 25 and 50°C.

Table 2. Parameters for Fitting Adsorption Isotherms

BDDT Isotherm Parameter	25°C	25°C*	50°C	50°C*
A	0.010659	0.010583	0.010700	0.010176
B	4.00000	4.0238	4.00000	4.272
C	25.3140	26.0535	13.0021	16.8951
D	60.9177	62.8668	47.5814	55.3134
SSD	7.7E-6	7.6E-6	9.1E-6	4.5E-6

The BDDT isotherm is:

$$q=\frac{ACX\{1+B[(D-1)X^{B-1}+DX^{B+1}-(2D-1)X^{B}]-X^{B}\}}{(1-X)[1+(C-1)X+C\{(D-1)X^{B}-DX^{B+1}\}]}$$

X = RH; A = saturation coverage; B = no. of monolayers at saturation; C = Henry's coefficient; D = energy of adsorption term

Dubinin-Astakhov Equation (Eq. 1)

$q_1 = 32.1231$ kmol/m$_s^3$
$q_2 = 8.5193$ kmol/m$_s^3$
$E_1 = 3.4434$ kJ/mol
$E_2 = 10.931$ kJ/mol
SSD = 0.0205 kmol/m$_s^3$

*Not constrained to integer value for parameter B.

monolayer filling (Henry's region lies roughly below RH = 2%), and is followed by the multilayer sorption up to around RH = 20% where an inflection point exists. The inflection indicates commencement of pore filling, which eventually dominates when the partial pressure reaches the effective vapor pressure for the average pore size. Although this condensation pressure is not obvious due to the heterogeneous nature of the amorphous silica gel, it may occur at the second inflection point, around RH = 30%. At RH = 60%, which is well below the saturation pressure, the uptake has reached more than 90% of the maximum capacity. This result is typical of any adsorbent with relatively small pores (micropores). As RH continues to increase beyond 60%, only the larger pores (larger than the critical pore size) seem to be involved in multilayer pore filling, while the global adsorbed-phase density approaches that of the liquid. The maximum capacity of 40.6 kmol/m^3·s was achieved at RH = 100%, the saturation pressure of water vapor.

During desorption at 25°C, that is, as RH decreases, no deviation from the adsorption isotherm was recorded in RHs above 65%. This clarifies the continuation of the multilayer adsorption process of the larger pores in higher pressure range immediately after the pore filling, as mentioned above. As RH is reduced below 65%, however, the desorption path remains linear for a while and departs from the uptake path. Therefore, the upper bound of condensation pressure exists at around RH = 65% for the larger pores (but still smaller than the critical size). A transition occurs at around RH = 50% and the desorption path suddenly drops rejoining the uptake path at about RH = 30%. The pressure corresponding to this is lower than condensation pressures of most pores associated with pore filling. Accordingly, the isotherm contains a hysteresis loop in the RH range from 30 to 65%. The hysteresis loop may be regarded as Type-H2 (IUPAC classification), since the desorption isotherm shows linearity at high pressures and is not parallel to the adsorption isotherm in the pore-filling region due to the broad pore-size distribution. This sorption hysteresis may be interpreted by conventional concepts associated with particular pore shapes (Gregg and Sing, 1982) or by a method based on pore network connectivity by the percolation theory (Seaton, 1991). The sorption behavior at 50°C is similar to that at 25°C; both exhibit the same magnitude of maximum capacity.

Figure 3a shows the adsorption data for both temperatures on the adsorption potential energy domain. The data follow a single characteristic curve with no apparent temperature dependence. The data have been fit by Eq. 1, the Dubinin-Astakhov equation:

$$q^* = q_1 e^{-(A/E_1)^2} + q_2 e^{-(A/E_2)^2} \tag{1}$$

where A is the adsorption potential energy or the differential molar work of adsorption defined by:

$$A = RT\ln(p^{sat}/p) \tag{2}$$

and the parameters, q_1 and q_2, are related to the total micropore volumes of individual sites, and E_1 and E_2 are the characteristic energies of adsorption. Table 2 lists the values of these parameters for the present system. This expression has a relatively simple form and accurately represents the characteristic curve

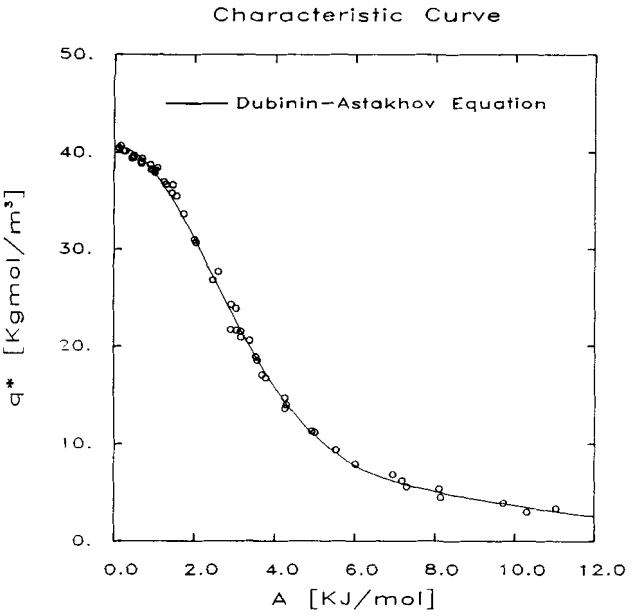

Figure 3a. Adsorption characteristics of the water vapor—silica gel system and the Dubinin-Astakhov equation.

See Table 2 for the parameters. The data plotted are from the sorption data at 25 and 50°C excluding those of desorption data exhibiting hysteresis.

of water vapor on regular density silica gel (van den Bulck, 1990).

Isotherms at various temperatures can be reproduced by Eq. 1 with the parameters obtained by a nonlinear regression. The results for temperatures 25 to 100°C are presented in Figure 3b.

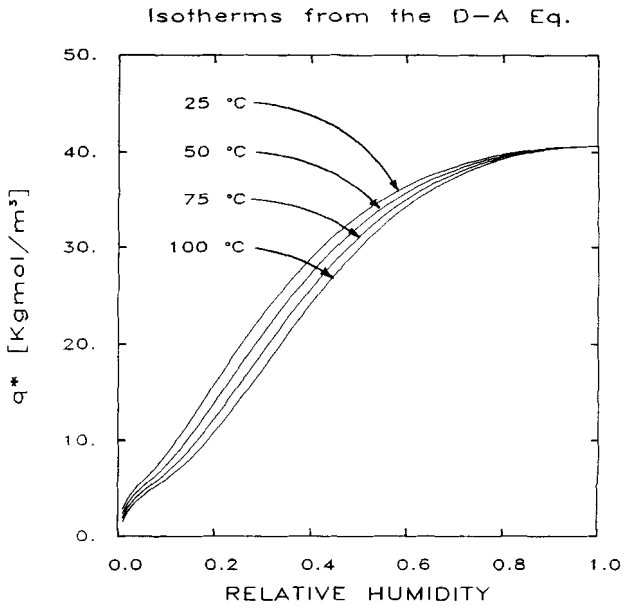

Figure 3b. Reproduction of adsorption isotherm of various temperatures from the Dubinin-Astakhov equation.

Isosteric heat of adsorption

The isosteric heat of adsorption, Q_{st}, is defined by:

$$\left.\frac{\partial \ln p}{\partial T}\right|_{q^*} = \frac{Q_{st}}{RT^2} \tag{3}$$

where q^* is adsorbed-phase concentration. Therefore, the isosteric heat of adsorption is inherently negative, and depends on temperature, the loading per unit volume of adsorbent, and the partial pressure of the adsorbate. The lefthand side of Eq. 3 can be obtained from the partial differential forms of Eq. 1:

$$\left.\frac{\partial \ln p}{\partial T}\right|_{q^*} = -\left.\frac{\partial q^*}{\partial T}\right|_{\ln p} \Big/ \left.\frac{\partial q^*}{\partial \ln p}\right|_{T} \tag{4}$$

Applying the chain rule to the partial derivatives of Eq. 4,

$$\left.\frac{\partial q^*}{\partial T}\right|_{\ln p} = \left.\frac{\partial q^*}{\partial A}\right|_{\ln p} \left.\frac{\partial A}{\partial T}\right|_{\ln p} \tag{5A}$$

$$\left.\frac{\partial q}{\partial \ln p}\right|_{T} = \left.\frac{\partial q}{\partial A}\right|_{T} \left.\frac{\partial A}{\partial \ln p}\right|_{T} \tag{5B}$$

Since $q = q(A)$ as shown in Eq. 1,

$$\left.\frac{\partial q^*}{\partial A}\right|_{\ln p} = \left.\frac{\partial q^*}{\partial A}\right|_{T} = \frac{dq^*}{dA} \tag{6}$$

Thus, combining Eqs. 3 to 6, a simple expression for the isosteric heat of adsorption is obtained,

$$Q_{st} = -\left.\frac{\partial A}{\partial T}\right|_{\ln p} \Big/ \left.\frac{\partial A}{\partial \ln p}\right|_{T} \tag{7}$$

On the other hand, the saturation pressure of water vapor at a temperature may be predicted from the Antoine equation,

$$\ln p^* = a - b/(T+c) \tag{8}$$

where the parameters are given by Dean (1974).

Substituting Eqs. 2 and 8 into Eq. 7, the isosteric heat of adsorption can be expressed as a function of adsorption potential energy and temperature as follows:

$$Q_{st} = -A - bRT^2/(T+c)^2 \tag{9}$$

The second term of Eq. 9 is merely the heat of vaporization of water, which can be obtained from the Clapeyron and the Antoine equations. Therefore, Eq. 9 shows that the isosteric heat of adsorption is the negative sum of adsorption potential energy and the latent heat of vaporization. Figure 4 indicates how the isosteric heat of adsorption depends on the concentration of the adsorbed phase at various temperatures, as calculated from Eqs. 1 and 9. It is noted that there is a singularity in the definition of Q_{st} given by Eq. 9 at zero coverage. That point, however, is irrelevant at all physically achievable conditions due to its logarithmic form.

Column dynamics

Comparison of Experimental and Predicted Results. Breakthrough experiments at room temperature for water vapor on silica gel were performed with various influent concentrations from RH = 6 to 80%. The experimental conditions are in Table 3 and typical results are shown in Figure 5. It is evident that the influent concentration changes not only

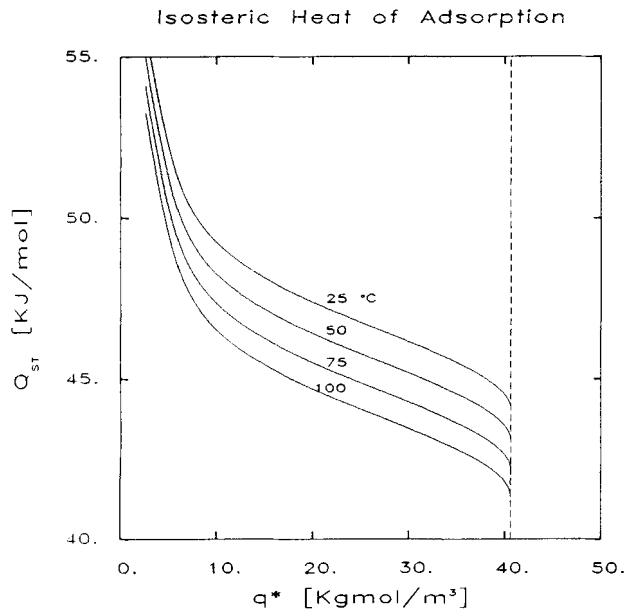

Figure 4. Isosteric heat of adsorption as a function of uptake at various temperatures.

See Eq. 9. Dashed line represents the maximum uptake for the system.

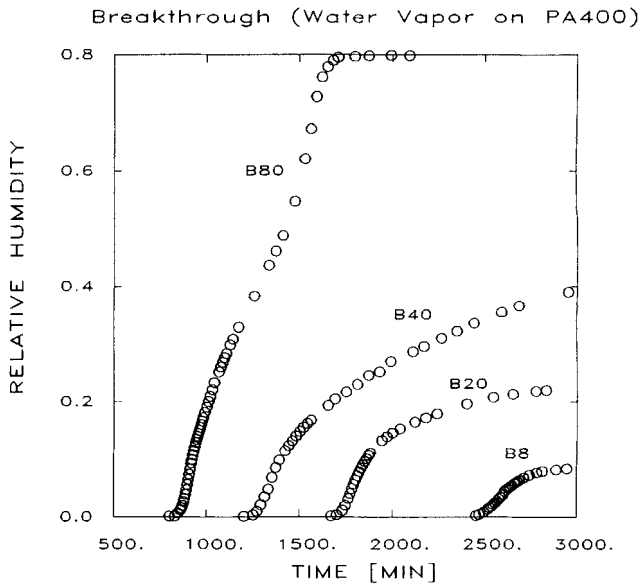

Figure 5. Typical breakthrough curves of water vapor-silica gel system at various influent humidities.

See Table 3 for the experimental conditions.

the breakthrough time but also the shape of breakthrough curve:

- A single shock wave exists at the lowest concentration.
- A combination shock wave and simple wave exists at the intermediate concentration.
- A complex wave exists at the highest concentration. It tends toward so-called "dual-shock waves" at the extremes of high and low concentration with an intermediate simple wave.

In two extreme cases, isothermal and adiabatic operations, straightforward methods for predicting breakthrough patterns have been suggested based on the shape of the equilibrium adsorption isotherm (Frey, 1990) and of the apparent adiabatic equilibrium (Basmadjian, 1990b) curves. In reality, most practical operations are nonisothermal, yet not adiabatic, and thus lie between the two extremes. The same is true for the present system of water vapor adsorbing on a fixed bed of silica gel in an uninsulated steel column.

In this case, both the isotherm shape and heat effects may play an important role in breakthrough behavior. Therefore, a more complete, yet still simple, model has been developed that includes an arbitrary isotherm with temperature-dependent parameters, as well as an allowance for heat transfer to the surroundings. These features were judged vital to predict the dynamic behavior of the present and most other nonisothermal systems. It could be applied to other fixed-bed adsorption processes such as PSA processes.

The basic assumptions made for the present model are essentially the same as given by Farooq and Ruthven (1990a):

- Two fluid-phase components, comprising an ideal gas mixture, are present.
- Only one component adsorbs, but with an arbitrary equilibrium isotherm (for example, Eq. 1).
- The linear driving force (LDF) approximation represents deviation from equilibrium between the fluid and solid phases.
- Axial dispersion and pressure gradients are negligible.
- Fast thermal equilibrium is established between fluid and adsorbent particles.
- Thermal exchange across the column wall is represented by the overall heat-transfer model.
- Temperature dependence of physical properties other than the isosteric heat of adsorption is negligible.
- Radial gradients of temperature and concentration are negligible (one-dimensional model).

Based on the above assumptions, mass balance for the adsorbed component in the fixed bed of adsorbent may be written as:

$$\frac{\partial c}{\partial t}+\frac{1-\epsilon}{\epsilon}\frac{\partial \bar{q}}{\partial t}+u\frac{\partial c}{\partial z}=0 \tag{10}$$

Similarly, the total energy balance is expressed in terms of an overall heat-transfer model:

$$\left(1+\frac{1-\epsilon}{\epsilon}\frac{\rho_s C_{p_s}}{\rho_g C_{p_g}}\right)\frac{\partial T}{\partial t}+\frac{1-\epsilon}{\epsilon}\frac{\rho_s}{\rho_g}\frac{Q_{st}}{C_{p_g}}\frac{\partial \bar{q}}{\partial t}+u\frac{\partial T}{\partial z}+\frac{2h/R}{\epsilon\rho_g C_{p_g}}(T-T_0)=0 \tag{11}$$

where the subscripts g and s refer to the gas and solid phases, respectively, and where h is the heat-transfer coefficient from the fluid to the wall. For C_{pg} and C_{ps}, the molar heat capacities of fluid and solid, average values over the experimental temperature range were used. On the other hand, h was estimated from an overall heat-transfer model [which considered the external wall heat-transfer coefficient to be governed by natural convection (Holman, 1986)], the thermal conductivity of the wall, and the internal effective heat-transfer coefficient (Suzuki, 1990). This approach was used to provide a good initial guess, which fell within about 40% of the value that best represented the present system. For example, for Run S1C, the predicted value of h was 5.10 W/m^2·K, while the actual value was observed to be 8.37 W/m^2·K.

The fluid-to-particle mass-transfer rate is represented by the linear driving force (LDF) approximation:

$$\frac{\partial \bar{q}}{\partial t}=k(c-c^*) \tag{12}$$

The mass-transfer coefficient, k, was obtained simply by parameter estimation. It was found to depend on flow rate, temperature, and geometry. Representative values are given in Table 3. For example, data from experiment B8 were analyzed with the model to determine the value of k for experiments S1C, S2C, and S3C. When the apparatus and flow rate changed, however, as in experiment U1T, a new value of k was determined to fit the data.

The adsorption isotherm is expressed in terms of adsorption potential, which itself is a function of gas composition and temperature (from Eq. 1):

$$\bar{q}=\bar{q}[A(c^*,T)] \tag{13}$$

Table 3. Breakthrough Experiments and Parameters for the Present Model

Run	RH Feed	Unit*	T	u	ϵ	k	h	$\rho_g C_{Pg}$	$\rho_s C_{Ps}$
	%		°C	m/s		1/s	W/m^2·s·K	J/m^3·K	J/m^3·K ($\times 10^{-6}$)
B8	8.0	a	23-25	0.125	0.62				
B20	22.5	a	23-25	0.125	0.62				
B40	40.0	a	23-25	0.125	0.62				
B80	80.0	a	23-25	0.125	0.62				
S1C	40.0	b	26	0.115	0.67	50.0	8.37	1,206.0	1.574
S2C	56.0	b	26	0.115	0.67	50.0	8.37	1,206.0	1.574
S3C	73.0	b	26	0.115	0.67	50.0	8.37	1,206.0	1.574
U1T	5.8	c	50	0.112	0.66	38.3	48.8	1,206.0	1.574
G1C	73.0	d	25	0.183	0.65	50.0	4.88	1,206.0	1.574

*See Table 1 for column dimensions.

The boundary conditions for breakthrough experiments are:

$$c(0,t) = c_F \tag{14a}$$

$$T(0,t) = T_F \tag{14b}$$

Similarly, the initial conditions of the breakthrough experiments are:

$$c(z,0) = 0 \tag{15a}$$

$$T(z,0) = T_0 \tag{15b}$$

$$\bar{q}(z,0) = 0 \tag{15c}$$

The conditions and parameters reflecting the experiments, which were also used in the computations, are listed in Table 3. The coupled nonlinear PDEs (Eqs. 10 to 12) were solved by a simple finite difference technique: the derivatives are approximated by backward differences on both time and position domains, and then the nonlinear nodal equations for c, $\bar{q}$, and T are computed by the interval-halving method. The solution technique is not very efficient compared to higher-order approximations for the same accuracy, as far as memory and computation time are concerned. Using a higher-order approximation with a restricted number of nodal points, however, tends to make the shapes of solutions stiff and distorted, and therefore was not pursued in this work. For this system, 200 nodes and single precision arithmetic were employed.

Theoretical and experimental breakthrough curves and temperature profiles are compared in Figures 6a and 6b. For the case of a very low influent relative humidity in Figure 6a, the breakthrough curve and temperature profile form a shock wave (or sigmoidal-shaped curve) and a Gaussian-shaped curve, respectively. This behavior is observed in many gas-phase breakthrough experiments at ambient temperature, because the gas pressures are far below the saturation pressures, and therefore isotherms are relatively simple.

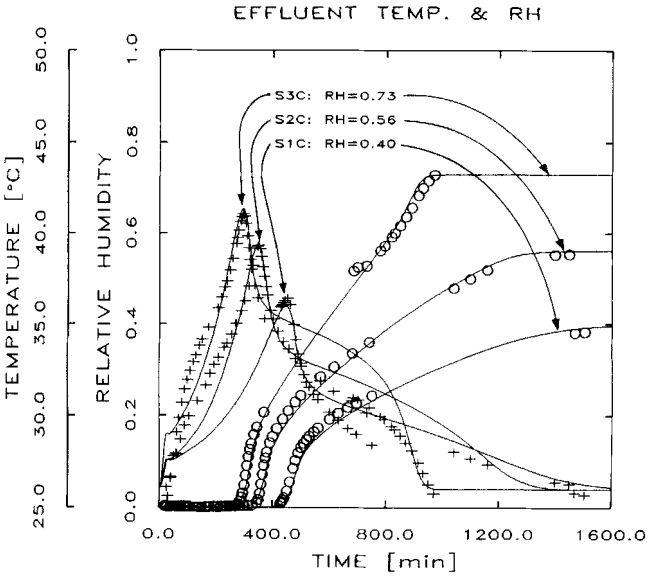

Figure 6b. Experimental and predicted effluent temperature and concentration: unusual patterns of column dynamics at intermediate and high influent concentrations, RH = 0.4, 0.56 and 0.73 at 26°C.

o, breakthrough data; +, effluent temperatures; —, solutions of this model.

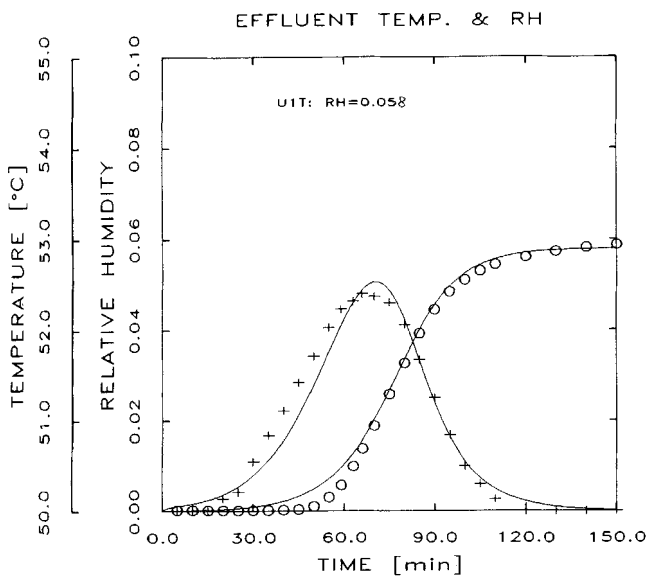

Figure 6a. Experimental and predicted effluent temperature and concentration: usual pattern of column dynamics at a low influent concentration, RH = 0.058 at 50°C.

o, breakthrough data; +, effluent temperatures; —, solutions of this model.

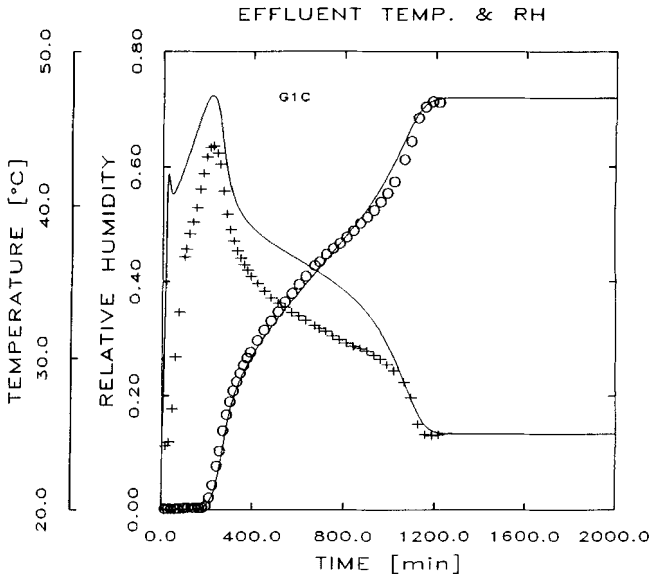

Figure 6c. Experimental and predicted effluent temperature and concentration: unusual patterns of column dynamics at high influent concentration, RH = 0.73 at 26°C.

o, breakthrough data; +, effluent temperatures; —, solutions of this model.

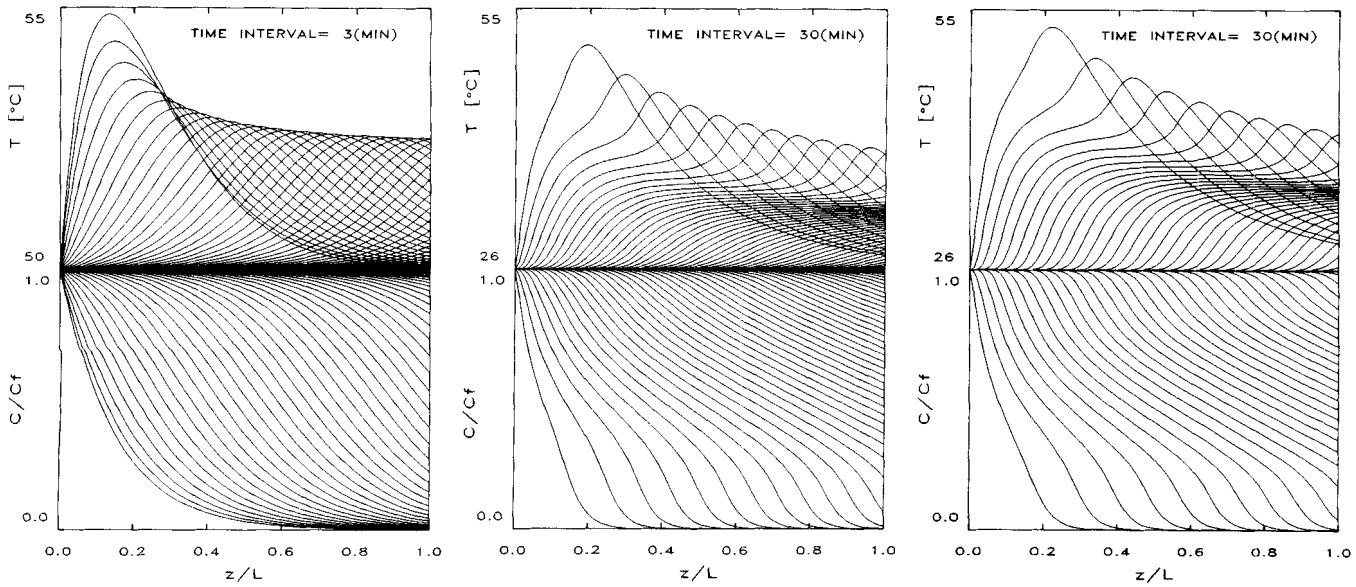

Figure 7. Concentration and temperature profiles in bed at various influent concentrations: (a) RH = 0.058 at 50°C (U1T in Table 3); (b) RH = 0.56 at 26°C (S2C in Table 3); and (c) RH = 0.73 at 26°C (S3C in Table 3).

In contrast, the breakthrough curves and temperature profiles for higher influent humidities are complex. Despite that, the experimental data are represented well by the theoretical predictions, as shown in Figures 6b and 6c. In particular, in Figure 6b the initial portions of the RH = 40% and 56% breakthrough curves are constant pattern (or shock) fronts that are followed by proportional patterns (or simple waves) until the curves reach their respective influent humidities. The case of RH = 73% (Run S3C), however, shows that a second shock front is formed as the feed composition is approached. An inflection point (at about 800 min) indicates the onset of the second shock front. The data in Figure 6c were obtained under similar conditions, but in a glass (rather than stainless steel) column. Because the column is nearly adiabatic and no gaps exist in the data (over 20 hours), the results confirm the observations in Figure 6b.

Effluent temperature waves rise steeply at the very early stages of uptake and reach peaks when the shock breakthrough fronts appear. After each peak, the effluent temperature drops sharply as the breakthrough curve rises. It is apparent from the variations of effluent temperature that the influence of heat, associated with the heat of adsorption in the column, plays an important role in determining the breakthrough patterns.

Figure 7 shows theoretical concentration and temperature profiles in the bed for the previously mentioned experimental conditions. In concentration profiles, Figure 7a for Run U1T (RH = 5.8% at 50°C) show nearly exponential decay along the column at early stages, followed by a shock wave (sigmoidal curve), which moves toward the outlet at a steady velocity. On the other hand, the temperature profiles initially rise sharply near the inlet, and then become broader as they propagate. The peaks occur as saturation of the adsorbent is approached at the influent concentration.

The case of RH = 56% at 26°C, Figure 7b, is slightly different. The concentration profiles start with initial patterns similar to that of RH = 5.8%, but soon evolve to a dual-shock pattern, which expands throughout the intermediate concentration range, instead of maintaining a constant pattern. Eventually, the higher concentration portion of the curve diminishes becoming nearly linear, while the lower shock wave is practically unchanged. The temperature profiles at RH = 56% also are not as simple as those at RH = 5.8%. Instead, sharp rises before the peaks propagate and decay very slowly as time elapses. The region where the profile is flat is due to both heat exchange with the surroundings and to relatively low uptake by the adsorbent, since the capacity is diminished due to the temperature rise. Similar profiles were obtained for Run S1C, and so the case is omitted in the figure. Figure 7c for RH = 73% exhibits similar behavior except that the upper shock wave does not dissipate as it propagates. It appears as a second constant pattern region in the effluent breakthrough curve. This was confirmed experimentally, and the results are shown in Figures 6b and 6c for experiments S3C and G1C, respectively.

Comparison of Isothermal, Adiabatic, and Experimental Results. In Figures 8a, 8b and 8c, predicted effluent temperatures and breakthrough curves that apply to the present experiments are compared to two extreme cases: isothermal and adiabatic systems at various influent concentrations. At the lowest influent concentration (RH = 8%), Figure 8a, the breakthrough curves of all the three cases are nearly indistinguishable, even though the effluent temperature profiles differ considerably. The isothermal profile is flat, the adiabatic profile is nearly a square wave, and the nonisothermal-nonadiabatic profile rises slowly and then drops sharply. At an influent concentration of RH = 40%, deviations of the breakthrough pattern from isothermal behavior increase: concentration breakthrough occurs earlier and the shape of the breakthrough curve becomes distended as the concentration rises toward saturation, as shown in Figure 8b. Conversely, for the case of RH = 73% in Figure 8c, the breakthrough curve begins earlier, but is sharper, because the equilibrium tendency is to form a dual-shock wave. A single-shock wave appears to be formed

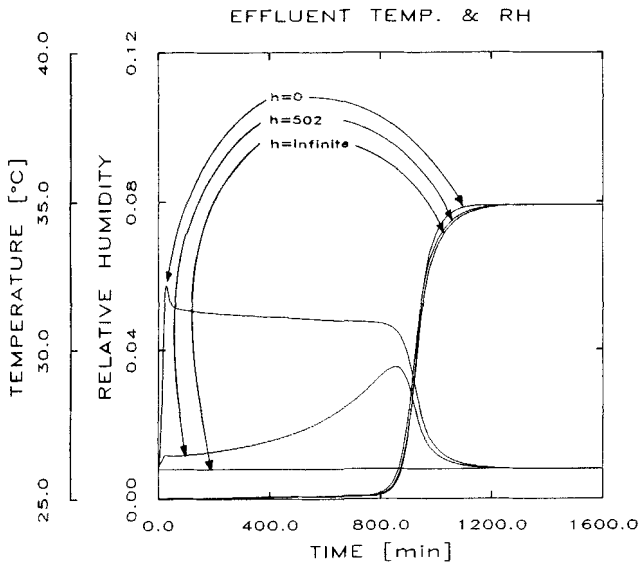

Figure 8a. Influence of nonisothermality on breakthrough at influent RH = 0.08.

Other conditions are the same as in S1C, S2C or S3C.

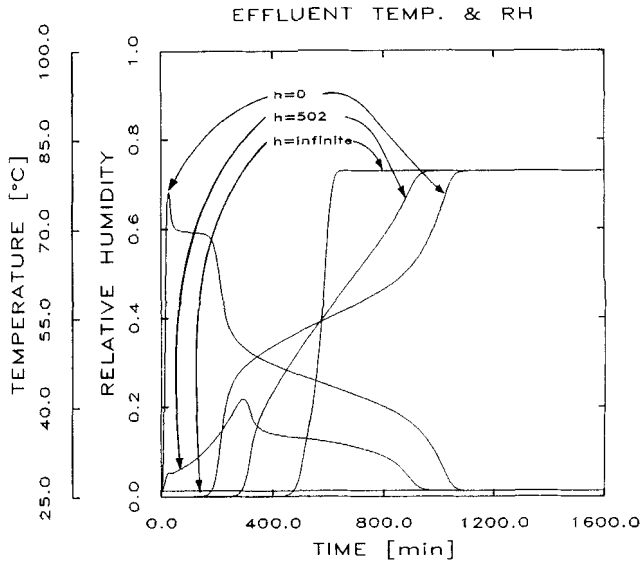

Figure 8c. Influence of nonisothermality on breakthrough at influent RH = 0.73.

Other conditions are the same as in S1C, S2C or S3C.

for the isothermal case, but on closer examination it may be seen to be a dual shock (the lower one exists up to about RH = 10% and the higher one begins at about RH = 50%). The adiabatic breakthrough curve forms an obvious dual-shock wave. The nonisothermal-nonadiabatic case lies between those two extremes.

Figures 9a and 9b show theoretical temperature and concentration profiles within the bed, as time proceeds, for the isothermal and adiabatic systems. The conditions shown are the same as for Run S3C except that the overall heat-transfer coefficient varies. These figures should be compared with Figure 7c, which represents the nonisothermal-nonadiabatic case

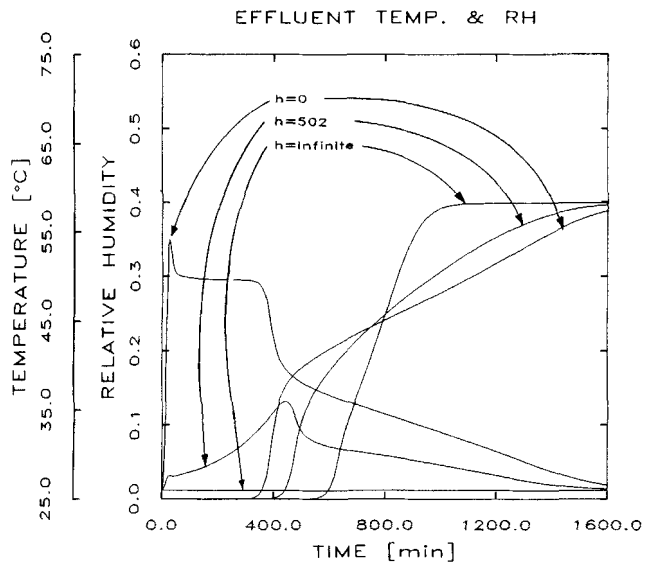

Figure 8b. Influence of nonisothermality on breakthrough at influent RH = 0.4.

Other conditions are the same as in S1C, S2C or S3C.

(Run S3C). For the isothermal system in Figure 9a, sharp concentration profiles move toward the effluent end of the bed exhibiting a constant pattern and constant velocity.

In contrast, for the adiabatic system in Figure 9b, more complex profiles exist. It is noted that there are two separate concentration regions: one that begins at the feed concentration and dissipates at about two-thirds of that value; the other that begins at about one-third of the feed concentration and dissipates at zero. These regions maintain constant patterns and displacement velocities. These two constant regions form a dual-shock wave in the breakthrough curve, as shown in Figure 8c. Since the velocity of the lower concentration is less than that of the higher concentration, the two concentration regions are eventually separated from each other as time elapses.

The temperature profiles, on the other hand, behave like the mirror images of the concentration profiles. This result can be observed from the fact that for an adiabatic system, Eq. 11 may be simplified eliminating the last term of the left-hand side, resulting in an energy balance analogous to the material balance, Eq. 10. Therefore, it is expected that in nonisothermal-nonadiabatic systems the temperature and concentration profiles would lie between the extremes of isothermal and adiabatic behavior.

These results show that for Type-VI isotherm systems, the formation of a dual shock in the breakthrough curve is more likely for a higher feed concentration and for an insulated system than for an isothermal system. In this case, the apparent isotherm exhibits more dramatic inflections and secondary saturation (above that of the monolayer) than the actual isotherm.

According to previous studies (Carter et al., 1968; Carter and Barrett, 1973; Basmadjian, 1980a,b), isotherms with relatively simple shapes such as Freundlich or Type II do not result in complicated uptake breakthrough patterns. In fact, our experimental and theoretical results with a Type-II adsorbent showed only a constant pattern profile, regardless of the inlet concentration and heat transfer through the column

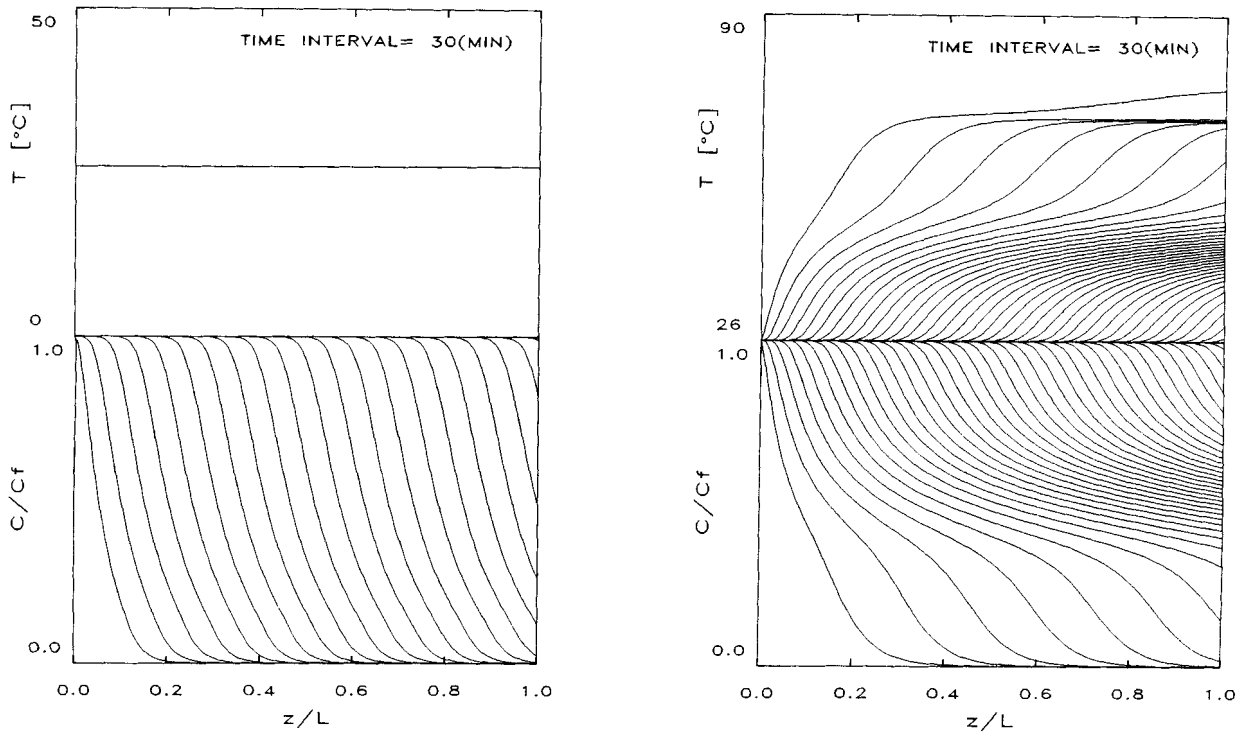

Figure 9. Concentration and temperature profiles in bed for isothermal and adiabatic systems:
(a) isothermal; (b) adiabatic ($h = 0$). All the conditions are the same as in S3C except the overall heat-transfer coefficient.

wall. Therefore, the dual-shock phenomenon exhibited in nonisothermal systems appears to require an inflection in the isotherm, just as for isothermal systems.

For isothermal operation with a Freundlich isotherm, the breakthrough curve always exhibits a constant pattern (or shock) regardless of the feed concentration. A Type-II system could show a combined shock + simple wave for a high-concentration feed. In addition, under isothermal conditions a Type-IV system could yield a dual-shock wave (Frey, 1990).

During nonisothermal operation, heat effects change the nature of the temperature profile. Usually, breakthrough starts earlier and has a long tail (Carter et al., 1968; Carter and Barrett, 1973; Basmadjian, 1980b). The earlier onset of breakthrough is due to the lower capacity of the bed at higher temperature, while the long tail indicates a complex coupling of heat transfer and adsorption. This is because the apparent equilibrium isotherm rises due to the gradually falling temperature (toward the feed temperature), characterized by relatively low heat-transfer coefficients and a high ratio of thermal capacities of the solid and fluid phases. For a Type-IV system, however, asymptotic behavior (after the exponential temperature increase) depends more strongly on the feed concentration than in a isothermal operation. The second inflection causes the formation of the second shock that cannot occur for simpler isotherms.

Summary

Adsorption equilibrium data at 25 and 50°C showed the maximum capacity of 40.6 kmol/m$_s^3$ and were represented well by the two-site potential model, the Dubinin-Astakhov equation. An expression for the isosteric heat of adsorption was derived from the D-A equation and the Antoine equation.

Various patterns of breakthrough behavior of water vapor on silica gel were observed experimentally, and they depended strongly on influent concentration. The breakthrough behavior can be described as three classifications: single-shock wave, shock + simple wave, and dual-shock wave; or in conventional terminology, constant pattern, constant + proportional pattern, and dual-constant pattern.

To predict breakthrough behavior, a nonisothermal dynamic model was developed, combining the linear driving force version of the continuity equation, the Dubinin-Astakhov equilibrium isotherm, and the isosteric heat of adsorption as a function of the temperature and uptake. The model represented the dynamic behavior very well over a wide range of influent concentrations (see Figure 6). It was noticed that a dual-shock wave, which is unusual in most other gas adsorption systems, was formed due to large heat effects accompanied by highly nonlinear adsorption equilibrium, especially for high influent concentrations. The theoretical adiabatic system in Fig. 9b shows the pattern clearly. In contrast, at intermediate influent concentrations, another type of breakthrough curve was observed, that is, a combined shock and simple wave. At very low influent concentrations, an ordinary symmetric, sigmoidal shock wave forms with no apparent effect of nonisothermality.

Acknowledgment

The authors are grateful to the Dow Chemical Company for supporting this work, particularly to Dr. Lanny Robbins who suggested the subject of this study. Suggestions provided by Professors Diran Basmadjian and Douglas Ruthven are also appreciated.

Notation

A = molar adsorption potential
c = concentration of adsorbate in gas
C_p = heat capacity
f = function
h = overall heat-transfer coefficient
k = film mass-transfer coefficient, vol.$_g$/(vol.$_g$ × time)
L = length of packed bed
p = partial pressure
p^{sat} = vapor pressure
$\overline{q}$ = moles of adsorbate per volume of solid at equilibrium with interfacial fluid concentration
q^* = moles of adsorbate per volume of solid at equilibrium
Q_{st} = isosteric heat of adsorption
R = gas constant
RH = relative humidity, p/p^{sat}
SSD = sum of squared deviations
t = time
T = temperature
u = interstitial velocity
y_i = mole fraction of component i
z = axial position within adsorbent bed

Greek letters

ϵ = void fraction of adsorbent bed
ρ = density

Subscripts

F = influent
g = gas phase
s = solid phase
0 = initial bed condition

Literature Cited

Basmadjian, D., "Rapid Procedures for the Prediction of Fixed-Bed Adsorber Behavior: 1. Isothermal Sorption of Single Gases with Arbitrary Isotherms and Transport Modes: Principles and Recommended Methods," *Ind. Eng. Chem. Process Des. Dev.*, **19**, 129 (1980a).

Basmadjian, D., "Rapid Procedures for the Prediction of Fixed-Bed Adsorber Behavior: 2. Adiabatic Sorption of Single Gases with Arbitrary Isotherms and Transport Modes," *Ind. Eng. Chem. Process Des. Dev.*, **19**, 137 (1980b).

Brunauer, S., L. S. Deming, W. E. Deming, and E. Teller, "On a Theory of the van der Waals Adsorption of Gases," *J. Amer. Chem. Soc.*, **62**, 1723 (1940).

Carter, J. W., "Isothermal and Adiabatic Adsorption in Fixed Beds," *Trans. Instn. Chem. Engrs.*, **46**, T213 (1968).

Carter, J. W., and D. J. Barrett, "Comparative Study for Fixed Bed Adsorption of Water Vapor by Activated Alumina, Silica Gel, and Molecular Sieve Adsorbents," *Trans. Instn. Chem. Engrs.*, **51**, 75 (1973).

Chase, H. A., "Prediction of Performance of Preparative Affinity Chromatography," *J. Chromat.*, **287**, 179 (1984).

Dean, J. A., ed., *Lange's Handbook of Chemistry*, p. 10, 11th ed., McGraw-Hill, New York (1974).

Dubinin, M. M., and V. A. Astakhov, *Izv. Akad. Nauk. SSSR, Ser. Khim.*, **5**(11), 17 (1971).

Farooq, S., and D. M. Ruthven, "Heat Effects in Adsorption Column Dynamics: 1. Comparison of One- and Two-Dimensional Models," *Ind. Eng. Chem. Res.*, **29**, 1076 (1990a).

Farooq, S., and D. M. Ruthven, "Heat Effects in Adsorption Column Dynamics: 2. Experimental Validation of the One-Dimensional Model," *Ind. Eng. Chem. Res.*, **29**, 1084 (1990b).

Frey, D. D., "The Entropy Condition for the Dynamics of Nonlinear Multicomponent Sorption in Porous Media," *Chem. Eng. Sci.*, **45**, 131 (1990).

Glueckauf, E., "Contributions to the Theory of Chromatography," *Proc. Roy. Soc.*, **A186**, 35 (1945).

Glueckauf, E., "Theory of Chromatography: II. Chromatograms of a Single Solute," *J. Chem. Soc.*, 1302 (1947).

Glueckauf, E., "Theory of Chromatography: XIII. Behavior of Wide Bands in Chromatographic Columns," *Trans. Farad. Soc.*, **60**, 729 (1964).

Holman, J. P., *Heat Transfer*, Chap. 7, 6th ed., McGraw-Hill, New York (1986).

Lee, H., and W. P. Cummings, "A New Method for Silica Gel Driers under Nonisothermal Conditions," *AIChE Symp. Ser.*, **63**(74), 42 (1967).

Ritter, J. A., and R. T. Yang, "Equilibrium Theory for Hysteresis-Dependent Fixed-Bed Desorption," *Chem. Eng. Sci.*, **46**, 563 (1991).

Ruthven, D. M., D. R. Garg, and R. M. Crawford, "The Performance of Molecular Sieve Adsorption Columns: Non-Isothermal Systems," *Chem. Eng. Sci.*, **30**, 803 (1975).

Seaton, N. A., "Determination of Connectivity of Porous Solids from Nitrogen Sorption Measurements," *Chem. Eng. Sci.*, **46**, 1895 (1991).

Suzuki, M., *Adsorption Engineering*, Kodansha and Elsevier Publishers, Tokyo and Amsterdam (1990).

van den Bulck, E., "Isotherm Correlation for Water Vapor on Regular-Density Silica Gel," *Chem. Eng. Sci.*, **45**, 1425 (1990).

Manuscript received Sept. 9, 1991, and revision received Feb. 27, 1992.